Cement and Concrete Research 39 (2009) 590–599

Contents lists available at ScienceDirect

Cement and Concrete Research

journal homepage: http://ees.elsevier.com/CEMCON/default.asp

Determination of the energy consumption during the production of various concrete recipes

B. Daumann *, H. Anlauf, H. Nirschl

University of Karlsruhe (TH), Institute for Mechanical Process, Engineering and Mechanics, D-76128 Karlsruhe, Federal Republic of Germany

ARTICLE INFO

Article history:
Received 27 June 2008
Accepted 21 April 2009

Keywords:
Powder mixing
Concrete mixing
Image analysis
Energy consumption
Application of energy

ABSTRACT

This article presents a report of the mixing of concrete on the laboratory scale in a single-shaft and twin-shaft mixer. For both mixers we selected five concrete recipes that cover a broad spectrum of concrete mixing techniques. The concrete recipes differ from each other amongst other things by virtue of the aggregate-sized distribution curves, water–cement ratio, flow properties, compressive strength and mixing times. The specifically volume-related application of energy – which is necessary for the homogenization of the particular recipe in the mixer – is an essential influencing variable.

The comparison of the specifically volume-related application of energy is possible only if the concrete recipes possess the same homogeneity. The time curve of the homogeneity plotted against the necessary mixing time indicates the mixing efficiency, which in turn is determined by an imaging measurement process. Comprehensive mixing experiments show that the resulting application of energy, measured via the current composition, does not provide sufficient information in order to define the actual homogeneity in the mixture. A method was developed for the purpose of comparing concrete mixtures based on various recipes with the same homogeneity in relation to the specifically volume-related application of energy. The particular application of energy can be determined via the required mixing time and the power output process in terms of time.

1. Introduction

Mixing of dry or moisturized powders is a unit operation in process engineering industry, and can be found in the construction-, food-, and pharmaceutical industries, as well as in other fields. This paper focuses on concrete mixers, of which there are two main categories. The first type of mixer produces concrete one batch at a time, while the second type produces concrete at a constant flow rate. The paper focuses on the discontinuous concrete mixer, in a single shaft- and twin shaft execution.

The user's objective when employing a charge mixer is to attain a defined homogeneity in the solids, to be mixed within the shortest possible mixing time. The change of mixing quality during the mixing time is described by the mixing efficiency. The mixing efficiency is determined in the classical manner. Representative solid samples are taken out of the mixing chamber and are analyzed outside for their composition. The conditions during the mixing process, such as power consumption, gradients of moisture or rate per minute etc. should remain unchanged. The boundary conditions influence the mixing efficiency [1]. The operator of a concrete plant is not so much interested in the mixing efficiency, but rather the mixer efficiency related to the product. The question here is how well a mixer can produce a uniform concrete from its constituents. The properties (specific concrete parameters) for fresh concrete such as the density of fresh concrete, the air content and the compressive strength etc. are often considered. The procedural method of determination of mixing quality can be found in the norm of RILEM [2], DIN EN-459-2 [3] and in [4].

Concretes of various categories of strength and quality are mixed and used in the industry daily by the ton. The mixing times are increased from a rather short 35 second mixing time for the traditional recipes to several minutes for the special concretes when large portions of fines components are involved. The flow rate of the concrete plants will reduce dramatically for high performance concrete. The various recipes are being studied by various research institutions of concrete with regard to strength, quality, and mixing time.

The development of the concrete recipes in the last 20 years according to [5] has developed from a four-component system (water, coarse aggregates, sand and cement) into multi-component systems since the early nineties. The addition of admixtures or synthetic micro silica makes the mixing task considerably more difficult, since these components have very large fine proportions, something that confronts some mixing processes with a difficult task. The present-day ultra high performance concrete, with compressive strengths of more than 200 N/mm^2, cf. [6], as compared to ordinary concrete with, for instance, a compressive strength of 20/25 N/mm^2, present modern mixing technique with increasing requirements. A further

* Corresponding author. Tel.: +49 721 608 4139; fax: +49 721 608 2403.
E-mail address: bjoern.daumann@mvm.uka.de (B. Daumann).

0008-8846/$ – see front matter © 2009 Elsevier Ltd. All rights reserved.
doi:10.1016/j.cemconres.2009.04.001

variety of concrete that has been of interest in research today is the self-compacting concrete described, for instance, in [7]. The concrete has a high flowability and can be placed without vibration.

Detailed information on the treatment and analysis of high performance concrete can be found in [8]. More specific parameters (rheology, microstructure) are available for measurement, but these simplify neither the treatment nor the analysis of high performance concrete.

The microstructure and rheological flow [9,10] of this high performance concrete is now more important than previously. In many cases the concrete quality can be recognized only in the finished product.

The quality of the concrete is critically determined by the microstructure. Based on the investigations, for instance, in [9], the microstructure of the concrete depends on the composition and the curing conditions as well as on the mixing method and the mixing conditions prevailing at the production site.

A recent publication attempts to solve this offline problem of concrete parameters by in-mixer measurements for describing mixture evolution during a concrete mixing process. The three inline measurements in [11] are power consumption, a concrete moisture sensor and a sensor for the rheology of concrete.

This paper describes an arrangement with the necessary application of energy for the purpose of concrete mixing based on various concrete recipes. The mixing time consists here of the sum of the loading period (dry mixing and wet mixing), the mixing period and a dispersion mixing period. It is well-known that the discharge and weighing periods also require energy, but these are disregarded in this paper.

In comprehensive experiments it becomes apparent that the comparison of different concrete recipes regarding the application of energy is only valid when the homogeneity of the different recipes is equal at the end of the mixing process. This is important for the integration of the power curve to determine the application of the energy. The load time of the aggregates is constant $t_{load} = 10$ s during the mixing experiments with the two shaft mixers.

Cazacliu and colleagues [12,13] show further details of new kinetic models for power consumption, using rheology and dimensional analysis to enhance the description. This paper does not include these parameters. Rather, a simple method should help determine the application of energy for a concrete recipe.

The method for assuming the homogeneity at the end of the mixing process is image analysis in this case. A helpful technique for the further evolution of this method of concrete recipe is [14] in which some cement was marked with a ferrous oxide. Using this analysis method, the homogeneity of a concrete mixture is determined from a portion of the power curve and the mixing efficiency. The practical user can produce and compare concrete mixtures with constant homogeneity if he knows the percentage energy portion in the range of the stationary power consumption. In a concrete plant it is not always possible to take a representative sample for the determination of homogeneity. Therefore, the determination of the mixing time, together with the enhancement of the mixing efficiency, using image analysis, represents a considerably more precise method for the determination of the homogeneity.

The method presented here is thus suitable for the determination of the mixing time for the attainment of a previously defined homogeneity. Of course it cannot replace any further testing methods, such as the flow consistency, homogeneity determination of the aggregates size distribution and the compressive strength determination.

These statistical aids are very precisely described in [15] which studied dry powder mixtures. The physical equation that characterizes the distribution of components (dispersion) in a powder mixing experiment is the Fokker–Planck-equation [16]. More information about this equation, its application and the necessary internal and boundary conditions by determination of the mixing efficiency can be found in [17–19].

2. Theoretical considerations for determination of the homogeneity

2.1. Theoretical considerations for determination of the mixing efficiency

The concrete norms such as RILEM document the statistical sampling of concrete samples in a very detailed manner. This chapter contains further details of the mixing efficiency. The statistic regarding the coefficient of variation and the empiric variance are contained in Appendix A. Sommer and colleagues [15,20] discuss taking samples of dry powders in some detail. The theory in Appendix A is based on only one powder component (the component of interest).

According to Sommer [15], the mixing efficiency – determined via the time span of the variance $\sigma^2(c_{P,i},t_M)$, according to Eq. (1) – consists of three variances. The variance of the measurement method $\hat{\sigma}_M$ contains the reproducibility and can be determined by preliminary experiments. As a rule, the latter should be so small that only the variance of the uniform random mixture σ_Z^2 will influence the system and so the variance of the measurement method $\hat{\sigma}_M$ is negligible ($\sigma_Z^2 >> \sigma_M^2$). The systematic variance σ_{Syst}^2 is thus a function of the time and, in its stationary state, has the value $\sigma_{Syst}^2 = 0$, that is to say, the mixing process is terminated. A longer mixing time does not improve the mixing quality,

$$\sigma^2\left(c_{P,i}, t_M\right) = \sigma_M^2 + \sigma_Z^2 + \left(1 - \frac{m_{E,T}}{m_P}\right) \cdot \sigma_{Syst.}^2. \quad (1)$$

Current spectroscopy measurement methods of [21–23], which can be employed only up to a certain sample volume, are employed in an attempt to reduce the effort required for the evaluation of the attainable mixing efficiency of continuous or discontinuous powder mixers. The difficulty inherent in all measurement methods relates to their calibration for each individual substance, something that is not possible in the case of many concrete recipes. Any missing calibration frequently leads to error sources in the determination of the concentration. Each of the referenced authors had studied powder samples and did not analyze fresh concrete samples.

Optical measurement methods with fiber-optical waveguides and CCD cameras were used by [24–28], each of which used image analysis in order to characterize the mixtures on the basis of particles with differing colors. Sampling from the mixing chamber could not always be dispensed within this case. For this purpose, however, the powder mixer had to be stopped briefly for the purpose of measuring the concentration distribution. This article therefore focuses on a method that relies on a determination of the concentration course and the mixing efficiency distribution by means of image analysis without sampling. A CCD video camera records the mixing process throughout the entire mixing time in order to thus determine the mixing efficiency. This measurement method offers the advantage that the camera can be used in a flexible manner when the structural size of the mixer or of the sample volume is changed. Furthermore, one can access the raw data as often as desired and at various times and under certain circumstances, in order to adapt the analysis method. Moving images of the mixing process, moreover, help gain an impression of the entire mixing procedure during the process.

2.2. Determination of mixing efficiency by means of image analysis

The digital images that were taken have a resolution of 720×576 pixels. The blue component (tracer) therefore cannot be resolved up to primary particle size. The tracer mass concentration is $\overline{c_{P,E}} = 0.74\%$: One can gain an impression of the mixing efficiency with a resolution of 366.8 mm^2 per sample. With increasing resolution, the details could, of course, be better recognized. However, disturbing non-homogeneities, such as reflections of particles or shadow formations caused by mixing tools and the trough edge, could then dominate the mixing efficiency. But the analyses showed that a

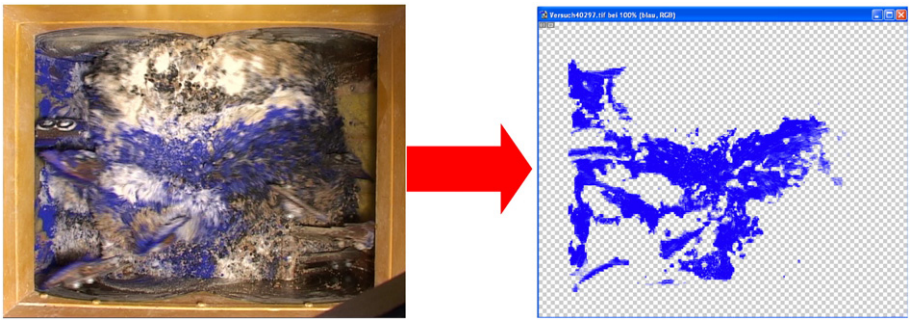

Fig. 1. Determination of the threshold value in the Adobe Photoshop® CS2 (a), original image, (b) separated fraction.

resolution of 366.8 mm^2 is entirely sufficient to describe the mixing efficiency for the purpose of characterizing the homogeneity. The individual digital images result from an image rate of one shot per second.

The individual images are finished in the Adobe Photoshop® CS2 such that only the blue component is preserved after a threshold value has been set. In the image analysis, the threshold value defines the differentiability between the tracer and the model mixture. Preliminary experiments are used to define the threshold value of individual command sequences that no longer need to be modified during the actual experiments. Figs. 1 and 2 show the method for separating the blue component for the single-shaft mixer and twin-shaft mixer. The tracer component can be separated by enhanced image analysis of the tracer dye according to Fig. 1a,b. More information about the using image analysis may be found in Appendix A or in [29].

3. Choice of the tracer

For these investigations, we used special colored particles as tracers, which clearly differ from the other aggregates in the mixing chamber. The same pigments, but with different properties were likewise used in [30]. Hence, ultramarine is chosen, as its density; mean particle diameters are very close to those of cement. In accordance with a recommendation of the producer Scholz, a concentration range of $\overline{c_{P,E}} = 0.5\%–1\%$ (related to the total quantity) was employed, so that the product properties of the mixing material (compressive strength, flow properties, etc.) would not be excessively influenced by the coloration with the pigment. In the concentration intervals of ultramarine blue described, compressive strength experiments with typical concrete mixtures were carried out. Only in the range from $\overline{c_{P,E}} = 0.5\%–1\%$ does the compressive strength demonstrate a minor influence. The tracer mass concentration is $\overline{c_{P,E}} = 0.74\%$. The compressive strength is not higher than 3–5% of the normal compressive strength.

The tracer used here is not intended to serve for staining a certain particle fraction or for marking it; instead, the tracer is used as a substitute for the one component that is difficult to mix. In this study, the tracer replaces the cement to a certain extent in order to visualize the real mixing behavior with the concrete recipe. The actual mixture thus consists of the tracer and the concrete recipes that will be described below.

As pigment, we used ultramarine blue because it behaves in a manner very similar to the cement with regard to density, particle size, flow behavior, sphericity, and the consolidation behavior of the solids. The pigment permits a differentiation in the image analysis program and almost completely retains its color spectrum in the concrete mixture. As the mixing time progresses, the tracer is distributed homogeneously in the entire mixing chamber and thus permits a resolution of the mixing process in terms of time.

The particle size distribution of cement and ultramarine blue is measured with the help of laser diffraction. The particular particle sizes x_{10}, x_{50}, and x_{90} then result from the sum distribution Q_3 according to Table 1. The color pigment has a narrower particle size distribution than does the cement. Wider particle size distributions however were not available commercially. The non-dimensional characteristics Hausner-ratio H and Carr-index C, according to [31,32], can be determined via the determination of the powder density ρ_S, the bulk density ρ_B, and the tapped density ρ_T. These parameters describe the densification behavior of fine powders. Here, the Hausner-ratio $H \geq 1.15$ and the Carr-index $C \geq 25\%$; therefore, according to the definition of both authors, these are bulk goods with a restricted or cohesive flow behavior. The sphericity Ψ of the two components, amounting to about $\Psi \approx 0.8$, differs only to a slight extent.

The flow properties of dry and moist solids were determined in analogy to the analysis method according to [33] in a Jenike-shear cell. Fig. 3 illustrates the experimental results. The flow site, that illustrates the shear stress τ_N plotted against the standard stress σ_N, shows that the flow behavior of the pigment ultramarine blue can be compared to that of cement. The mass of the cement or the pigment is constant in each case while the water volume varies. As the water–cement ratio rises, so do also the shear stresses due to the internal friction of the capillary cohesion forces. The shear stress declines again only with water–cement ratio of $W/C \geq 25\%$, which points to a resultant improved flow behavior. This means that the cement has attained its heat saturation at about $W/C \sim 25\%$ and the freely movable water

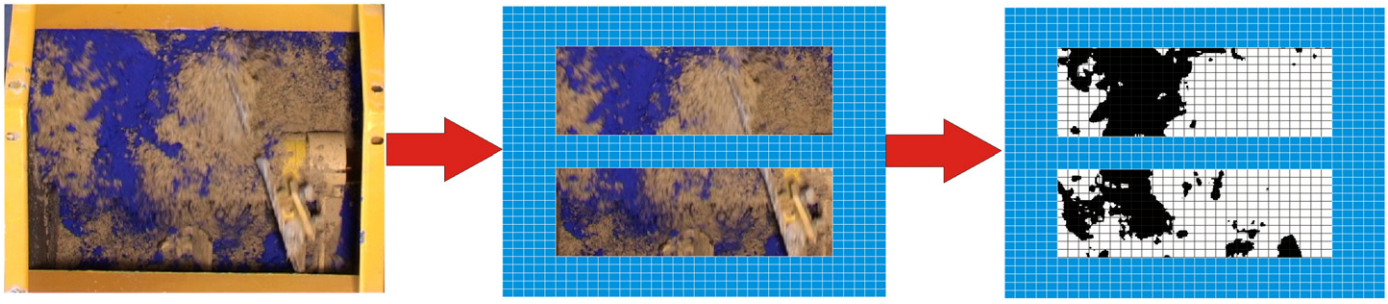

Fig. 2. Basic imaging during segmenting of the digital images, using the example of the single-shaft mixer.

Table 1
Powder properties.

	Ultramarine blue	Cement
Color	Blue	Grey
Particle diameter x_{10}	10.5 μm	2.4 μm
Particle diameter x_{50}	16.2 μm	13.51 μm
Particle diameter x_{90}	20.5 μm	82 μm
Powder density ρ_S	2400 kg/m^3	2900 kg/m^3
Bulk density ρ_B	990 kg/m^3	1200 kg/m^3
Tapped density ρ_T	1400 kg/m^3	1750 kg/m^3
Hausner-ratio H	1.41	1.45
Carr-Index C (%)	29.3	31.4
Sphericity Ψ	≈0.82	≈0.78

increases the flowability. Measurements with the shear cell are no longer possible in this case.

4. Experimental set-up

The experiments were performed on a horizontal single-shaft and a twin-shaft mixer provided by Firma ELBA-Werk Maschinen GmbH. The volume of the single-shaft mixer according to Fig. 4 is $V=60$ L. The volume of the twin-shaft mixer according to Fig. 5 is $V=120$ L. The mixers have spiral mixing tools that move horizontally. It is characteristic of the twin-shaft mixer that the two mixing tools overlap in the middle part of mixing chamber. The mixing tools of the twin shaft mixer move in opposite directions towards each other. The product can be conveyed from the outer edge of the trough toward the interior or from the interior to the outer edge. In the single-shaft and twin-shaft mixer, the wall-mounted mixing tool has a diameter of $D_W=550$ mm. The length to diameter ratio between the drum diameter and the length is $D_T/L\approx1$ for the single-shaft mixer and about $2D_T/L\approx2$ for the twin-shaft mixer. The filling ratios φ were $\varphi\approx50\%$. The rate per minute (rpm) for the single-shaft mixer n can be adjusted up to 75 rpm; for the twin-shaft mixer it is 49 rpm. A constant rpm of $n=20$ rpm is set for the performance of the mixing trials. In average mixing jobs, the mixing times are about $t_M\approx35$ s according to [2].

The mixing process can be observed or recorded continually if a video camera is positioned perpendicularly above the mixing chamber. The Sony VX2100E video camera employed here has a resolution of 720×576 pixels with an image rate of 30 images per second. A 1000 W Halogen lamp illuminates the mixing chamber in such a way that the formation of shadows by the mixing tool and the trough edge according to Fig. 6 is greatly reduced and the influence of outside light is minor. The loading of the mixers with the coarse aggregates, sand and cement etc. will be dosed over a

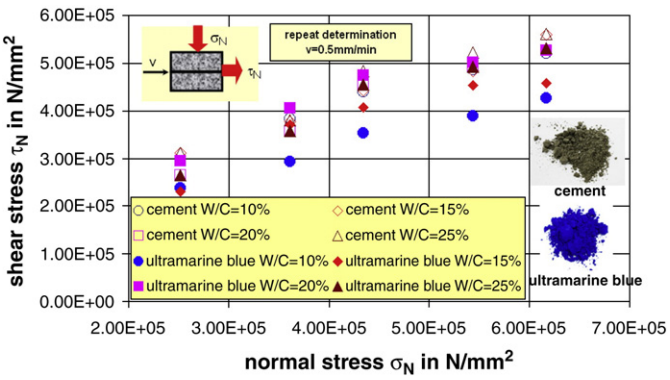

Fig. 3. Flow site determination according to Jenike.

Fig. 4. View of mixing chamber.

purpose-built breadboard construction. The breadboard operates fully automatically.

5. Concrete recipes examined

The selected recipes cover a broad spectrum of concrete mixing technique according to Table 2. This involves a test concrete (PB2-concrete), a self-consolidating concrete (SCC), two transit-mixed concretes (C25/30-concrete and C50/60-concrete), and an ultra high performance concrete (UHPC). Fig. 7 illustrates the aggregates size distribution (grading curve), such as sand, gravel, split, and basalt. The distribution of the fine particle is illustrated in Fig. 8, such as the cements, tracer or the micro silica.

6. Results

6.1. Preliminary experiments by the determination of the application of energy

The power output process must be determined as a function of the mixing time t_M in order to determine the specifically volume-related application of energy E_V. The various components of the concrete recipes produce different possibilities for charging the components into the mixing chamber. As a rule, the dry components are prepared in the mixing chamber and only then, after a defined pre-homogenization time, are the liquid components (water, admixtures)

Fig. 5. View of mixing of ELBA-Laboratory single-shaft chamber ELBA and Laboratory mixer twin-shaft mixer.

Fig. 6. Mixer and camera.

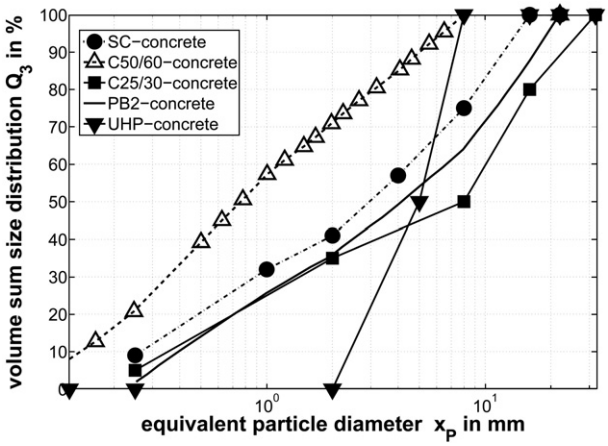

Fig. 7. Volume sum distribution Q_3 (aggregates size distribution) of aggregates.

added. Comprehensive series of experiments, however, showed that one can measure the influence of the charging sequence of the dry components upon the mixing efficiency.

Using the example of the single-shaft mixer, Fig. 9 shows three production runs with variation of the charging sequence for the concrete recipe of the ultra high performance concrete (UHPC). The volumes of the fresh concrete from the single-shaft and twin-shaft mixer are not identical; the power output process and the mixing time are therefore plotted in a volume-related manner. Thereby, the mixing time will be divided through the volume $V = 0.06$ m^3 of the single-shaft mixer. The twin-shaft mixer volume is $V = 0.12$ m^3 per batch of concrete. A dosing device facilitates the charging of the components in a previously determined sequence.

In dosage 1, the admixture was added directly with the water after charging the cement with the aggregates (basalt, microsilicate, microwirefiber, silica flour and silica sand). In the ultra high performance concrete, during the addition of the liquid with admixture, on account of the effect of the capillary cohesion forces, one can recognize an outward jump that was also documented in [5]. The power consumption drops considerably only when the admixture reacts with the cement and when the filling level in the powder mixer declines. The reaction of the cement with the admixture was brought out clearly with the help of dosage 2. Here, the aggregates were charged with the admixture and the water simultaneously and the cement was charged only after 30–40 s. Due to the charging of the water with the aggregates, the power consumption is briefly greater than in the case of dosage 1 but then again drops faster. After the charging of the cement, the power consumption increases again so that a delayed cement charge will result in an extension of the mixing time.

The influence of the admixture can be explained in dosage 3. Here, the aggregates were charged with water and cement with admixture was dosed into the mixing chamber after about 30–40 s. The liquid was balanced out after the aggregates had been charged and this was indicated by a decline in the power output peak. An almost constant power consumption results after a mixing time of about 100 s by adding the cement and the admixture. The power consumption declines in proportion to the filling level in the mixer. This is caused by the fact that the admixture, along with the reaction with the cement, must also be distributed in the entire mixture, so that the mixing time is considerably extended. One can clearly see that the dosing sequences critically influence the power output development. The reproducibility of the individual variations of the dosing sequences of course becomes difficult as a result of manual dosing. Dosage 1, that is to say, the charging of the dry component with subsequent water or admixture charging, was considered most suitable for further investigations because the reproducibility of this variant proved to be very reliable even in case of manual charging.

6.2. Concrete experiments by the determination of the power curves

During the measurements of the power consumption the idling speed is not included in the absolute values of power. Figs. 10 and 11 show five power output curves for different concrete recipes for the

Table 2
Selected concrete recipes, giving the component mass with relation to a cubic meter of fresh concrete.

Compositions	PB2-concrete	SC-concrete	C25/30-concrete	C50/60-concrete	UHP-concrete
Cement (CEM I 32.5R or CEM I 42.5R)	370 kg/m^3	350 kg/m^3	280 kg/m^3	450 kg/m^3	582 kg/m^3
Aggregates (sand, gravel, split, or basalt)	1789 kg/m^3	1617 kg/m^3	1806 kg/m^3	1715 kg/m^3	714 kg/m^3
Fly ash	–	200 kg/m^3	60 kg/m^3	–	–
Admixture	–	5.4 kg/m^3	1.4 kg/m^3	–	35.9 kg/m^3
Synthetic microsilica	–	–	–	–	178 kg/m^3
Silica flour	–	–	–	–	458 kg/m^3
Silica sand	–	–	–	–	355 kg/m^3
Microwirefibers	–	–	–	–	196 kg/m^3
Water	155 kg/m^3	175 kg/m^3	182 kg/m^3	225 kg/m^3	170 kg/m^3

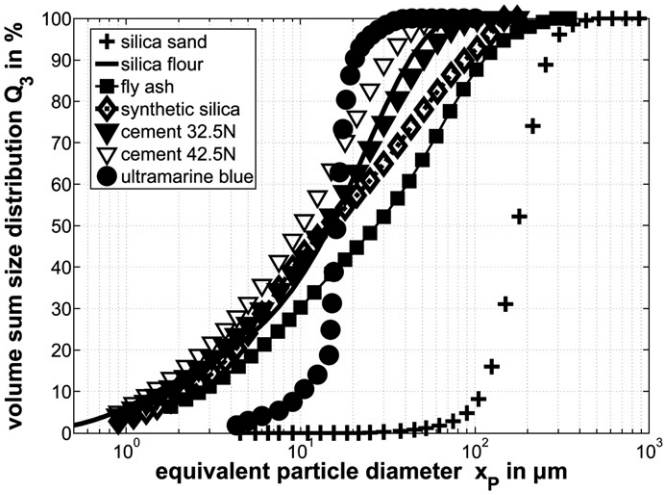

Fig. 8. Volume sum distribution Q_3 (particle size distribution) of fine used particles.

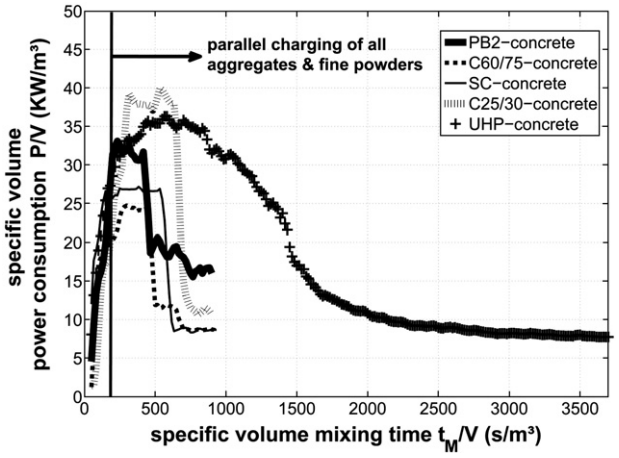

Fig. 10. Power curves for five concretes — single-shaft mixer.

single-shaft and twin-shaft mixer. In both figures, the effective power output P and the mixing time t_M are related to the volume V of the fresh concrete. We get the pertinent power output curves for the test concrete (PB2), the self-consolidating concrete (SCC), the two transit-mixed concrete (C50/60, C25/30), and the ultra high performance concrete (UHPC). For making ultra high performance concrete, the mixing time for both mixer types is longest when compared to the other recipes.

The power curves according to Fig. 10 for the single-shaft mixer show the highest power output requirement for the four standard recipes (PB2, C50/60, C25/30, SCC) after charging the dry components. The maximum power output peak for the dry mixing area in the case of the single-shaft mixer is a function of the maximum aggregates size (see also the aggregates size distributions of the individual concretes in Fig. 7). In the single-shaft mixer, a considerable portion of the aggregate friction takes place both along the trough wall and in the bulk pile, as a result of which the required power output is also increased with increasing rough substance portion in the aggregate size distribution. The relatively narrow gap between the mixing tool and the mixer wall of the single-shaft mixer means that individual aggregates can become stuck, something that results in a high aggregate friction along the trough wall. After charging water and possibly admixtures, the power consumption, after a reaction and stay time in the heap, drops definitely all the way down to liquid balance. The power output increase after the addition of water and admixture, recognizable in Fig. 9, also occurs in the case of the ultra high performance concrete which, in this case, has already taken place at the start of the mixing action.

In the twin-shaft mixer, the maximum power peaks in the dry heap are considerably closer together. One cannot recognize the influence of the rough portion because the main resistance of the mixer is in the area where the two mixing tools overlap. Adding the liquid results in a slight increase in the specific volume power consumption until the liquid balance has taken place in the entire mixing chamber.

The two mixing tools always lift the same volume of product per revolution. Therefore, the rising cohesive force – except for the ultra high performance concrete – exerts only little influence on the specific volume-related power consumption. In the single-shaft mixer, the specific volume mixing time t_M/V and the specific volume power consumption P/V is greater than in the twin-shaft mixer.

6.3. Determination method for the volume-related application of energy

The specifically volume-related application of energy cannot be determined directly from the power curves of the single-shaft and twin-shaft mixer because the mixing time necessary for a homogeneous mixture is not known. Some authors have studied this problem before. Chopin and colleagues [34,35] propose a method for the determination of the application of energy under a power consumption curve. The solution for this problem is the definition of the stabilization mixing time. That is an abort criterion when the concrete mixing is finished. This part of the power curve is called the "macro mixing" or homogenization time. Another publication [36] has discussed the problem that high performance concretes require more

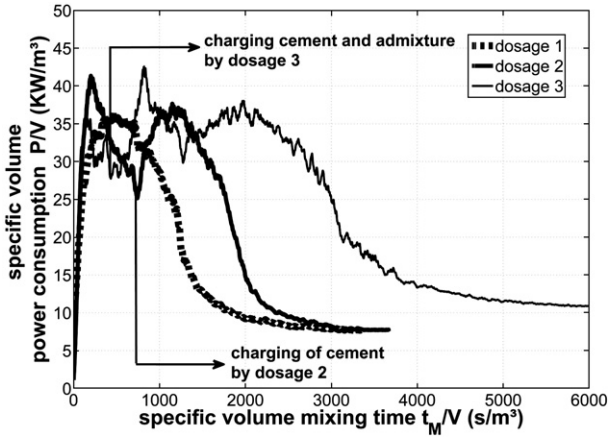

Fig. 9. Differing dosing sequences for ultra high performance concrete.

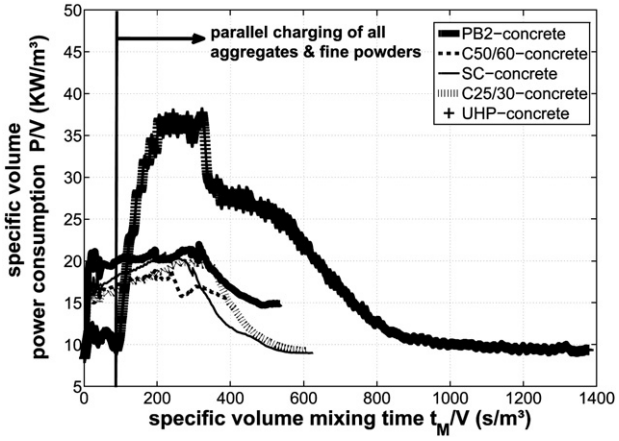

Fig. 11. Power output curves for five concretes — twin-shaft mixer.

mixing time than only the stabilization mixing time. This time is defined as "mixing dispersion".

The power consumption does not permit any statement as to the quality of the various concrete recipes in the mixing chamber. A comparison of the necessary specific volume-related application of energy among the concrete recipes can be made only if the homogeneity is identical. The power output curve barely provides a hint as to any non-homogeneities in the entire mixing chamber. The specifically volume-related power consumption, determined as a function of the time, only represents an integral magnitude for judging the mixer at a certain point in time. With declining specific volume-related power consumption, one can, in the individual curves, recognize fluctuations that point to homogeneity differences. These homogeneity differences however cannot be analyzed in the curves so that local non-homogeneities cannot be determined via the power output, but rather via the mixing efficiency.

To determine the entire mixing time t_M, one must, therefore, subdivide the power curve into two mixing times, t_1 and t_2. The mixing time t_1 is the time needed in order to minimize the concentration gradients in the entire concrete recipe. This mixing time t_1 is compared with the stabilization mixing time in publication [34,35]. The mixing time t_2 gives the time the powder mixer needs in order to attain a defined homogeneity of a fine component (dispersion mixing) which is therefore difficult to mix. From [36] we know that the additional mixing time does not possess any benefits for the rheology of concrete. But this kind of determination allows a better comparison between the two concrete mixers, because the mixing behavior is different. From the integration of the specifically volume-related power curve and the determined mixing times, one can, according to Eq. (2), determine the specifically volume-related application of energy E_V by means of a simple addition of the two portions,

$$E_V = E_{V_1} + E_{V_2}$$
$$E_V = \frac{1}{V}\cdot\left(\sum_0^{t_1} P(t_M)\cdot dt_M + \sum_{t_1}^{t_2} P(t_M)\cdot dt_M\right) \quad (2)$$
$$\text{Total mixing time}: t_M = t_1 + t_2$$

Fig. 12 shows the two mixing areas and mixing times. The problem now is to determine the exact moment at which the mixing time t_1 is terminated and the mixing time t_2 commences. This calls for a determination of the rise of the power output curve during a specific time interval of one second, that is to say, when the pattern of the curve becomes stationary. A maximum change of the power output curve in terms of time of $P'(t_M) = \Delta P/\Delta t_M \le 1\cdot 10^{-2}$ KW/s was determined as criterion for this purpose. This criterion among other things results from

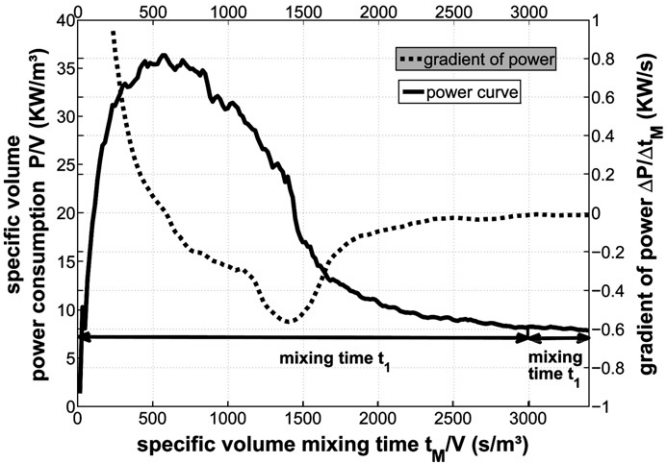

Fig. 12. Power curve of UHPC in single-shaft mixer with particular break-off criteria.

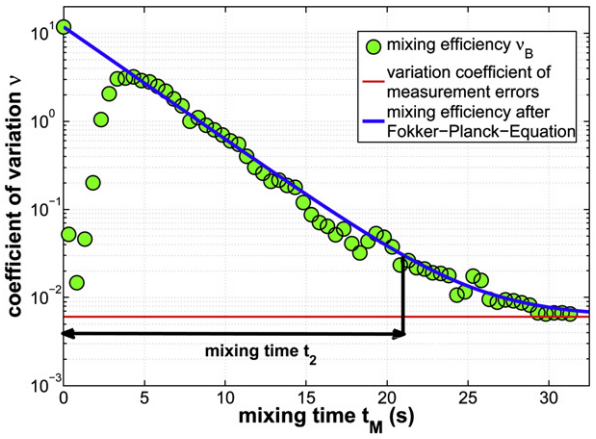

Fig. 13. Mixing efficiency for ultra high performance concrete in single-shaft mixer.

the fact that the minimum resolution of the power output measurement is 0.01 KW. A data evaluation, however, shows meaningful results only when the raw power output data are refined by a moving average value according to [37] and in Appendix A.

To be able to compare the homogeneity of the various concrete and mixer types, the mixing time t_2 is determined after determination of the mixing efficiency under constant experimental conditions. A tracer component is charged as horizontally convert on the surface whose flow behavior is almost identical with that of the cement employed here, as described earlier. Via this tracer marking and the analysis of the digital images, one can then determine the mixing efficiency as a function of the mixing time for each recipe. A mixing time t_2 is attained when a variation coefficient of $v \le 0.03$ for the cement particles as developed according to Fig. 13. According to RILEM, this corresponds to a High Performance Mixer (HPM). In Fig. 13, $N_P = 400$ samples were analyzed in a sample quantity m_P for the fine component of $m_P \approx 2.8$ g. The detail of this determination method will be found in [29].

From the mixing efficiency one can then, according to Eq. (1) from the Fokker–Planck-equation, calculate a dispersion coefficient. This physical equation can only be used if pure dispersion properties exist. The solution of this physical equation is an exponential curve with one fitting parameter. This mixing time t_2 according to Fig. 13 is plotted in the line of the power output curve in Fig. 12. The mixing time t_2 is also marked with the break-off criterion according to Fig. 13.

Knowing the mixing time t_1 from the power curve and the mixing time t_2 from the mixing efficiency of the five concrete recipes, one obtains the specifically volume-related application of energy necessary for a homogeneous mixture through the integration of the power output curves.

6.4. Specially volume-related application of energy by the two concrete mixing types

Table 3 shows the terminally-dimensioned, specifically volume-related power consumptions. $E_V/E_{V,UHPC}$ stands for the entire necessary specifically volume-related application of energy E_V of the specified concrete recipe related to the recipe of the ultra high

Table 3
Non-dimensional specifically.

Concrete recipe	Single-shaft mixer		Twin-shaft mixer	
	$E_V/E_{V,UHPC}$	E_{V2}/E_V	$E_V/E_{V,UHPC}$	E_{V2}/E_V
C25/30 concrete	35% ± 1.1%	21% ± 2.4%	61% ± 2.0%	12% ± 1.0%
C50/60 concrete	32% ± 0.9%	15% ± 1.2%	39% ± 2.0%	15% ± 1.6%
PB2 concrete	39% ± 2.1%	23% ± 2.1%	56% ± 2.5%	11% ± 0.9%
SC concrete	42% ± 1.2%	14% ± 1.1%	62% ± 7.7%	12% ± 0.9%
UHP concrete	100% ± 8.4%	5% ± 0.6%	100% ± 9.1%	11% ± 0.9%

performance concrete $E_{V,UHPC}$, for the single-shaft and twin-shaft mixer. In the single-shaft mixer we note that the individual specifically volume-related applications of energy $E_V/E_{V,UHPC}$, show very similar values for the standard concretes. Almost three times as much energy is necessary for preparing homogeneous, ultra high performance concrete. If the volume-related application of energy E_{V2} of a recipe, necessary for the attainment of a defined homogeneity – after a constant power consumption has already been attained (mixing time t_2), – is related to the entire specific volume application of energy E_V for the production of the homogeneous mixture (from the mixing times t_1 and t_2), then one can see that a by no means negligible part of the total energy is necessary in order to obtain the same required homogeneity among the individual concrete recipes. As shown in the table for the illustrated applications of energy E_{V2}/E_V in the single-shaft mixer, 14% to 23% energy is needed to attain an identical homogeneity. In the single-shaft mixer, the ultra high performance concrete only needs about 5% of the total specific volume-related application of energy.

Comparing the values of $E_V/E_{V,UHPC}$ for the single-shaft and twin-shaft mixer, one can determine that the percentage energy expenditure for the twin-shaft mixer is closer to the energy requirement of the ultra high performance concrete. Except for the C50/60-concrete, that contains small parts of rough products in the aggregate size distribution, the necessary applications of energy are very similar. A difference can be found when one compares the values of E_{V2}/E_V among the two mixers. The values in the region of the stationary power consumption are lower for the twin-shaft mixer than for the single-shaft mixer. The latter are roughly 12% to 15% of the necessary specific volume application of energy. In the twin-shaft mixer this energy has already been charged into the mixing material in the mixing area due to the higher power consumption in which the mixing time is located. Therefore, the residual energy portion necessary to attain a defined homogeneity is smaller than in the single-shaft mixer.

Using the analysis method presented here – where the homogeneity of a concrete mixture is determined from a part of the power output curve and a mixing efficiency – the practical user can make and compare concrete mixtures with constant homogeneity if he knows the percentage energy portion in the area of the stationary power consumption. In big systems it is not always possible to take a representative sample out for a homogeneity determination. Therefore, the determination of the mixing time t_2 from the mixing efficiency represents a considerably more exact method for the determination of the homogeneity.

7. Summary

This article explains in greater detail a procedure that facilitates a comparison of various concrete recipes with relation to their mixing homogeneity. An evaluation of the homogeneity is impossible on the basis of the power output curve. The mixing quality can be determined only on the basis of the mixing efficiency. The determination of the mixing efficiency in this study facilitates an imaging measurement method in which a dye pigment as tracer visualizes the distribution of a component that is difficult to mix. The specific volume application of energy can be calculated via a defined break-off criterion from the power output curve that must be subdivided into two time segments. The first mixing time indicates the moment as of which the concentration gradients are balanced in the entire mixture. The second mixing describes the process up to the attainment of a homogeneous tracer component distribution. In comparing the standard concrete recipes it was found that, to attain a defined terminal homogeneity in both mixing time spreads during the mixing process, approximately the same amount of energy must be expended. The highest application of energy is necessary for the ultra high performance concrete, since this requires the longest mixing time. The energy portion that must be expended for a homogeneous mixture – after the power output curve has already passed into the stationary area – is considerably higher in the single-shaft mixer than in the twin-shaft mixer. The method presented here is thus suitable for the determination of the mixing time for the attainment of a previously defined homogeneity. Of course, it cannot replace any further testing methods, such as the dispersion measure, homogeneity determination of the aggregate size distribution and the strength determination.

Symbols

A_P	Sample size [pixel^2]
C	Carr index [%]
c_j	concentration of fractions j [–]
$\overline{c_{P,E}}$	target value of solid concentration [–]
$c_{P,i}$	solid concentration of a sample i [–]
D_T	drum diameter [m]
D_W	tool diameter [m]
E_V	specific volume application of energy [J/m^3]
H	Hausner-ratio [–]
i	number of samples [–]
L	length of drum [m]
$m_{E,T}$	mass of individual grain [kg]
m_P	sample quantity [kg]
N	number of time steps for data smoothing or linear Regression [–]
n	number of revolutions [s^{-1}, rpm]
N_P	number of samples [–]
P/V	specific volume-related power consumption [W/m^3]
P'	increase in specific volume-related power consumption [W/s]
Q_3	volume sum distribution [%]
s^2	empirical variance [–]
t_M	mixing time [s]
t_1	mixing time in non-stationary mixing area [s]
t_2	mixing time in stationary mixing area [s]
V	volume [m^3]
x_{10}	average particle diameter for $Q_3 = 10\%$ value [μm]
x_{50}	average particle diameter for $Q_3 = 50\%$ value [μm]
x_{90}	average particle diameter for $Q_3 = 90\%$ value [μm]
$x_{A,T}$	equal-surface particle diameter of a sphere of tracer [μm]
x_P	equivalent diameter of a screen mesh [μm]
$x_{V,T}$	equal-volume particle diameter of a sphere of tracer [μm]
x_V	equal-volume sphere [μm]
x_W	mass-related moisture [%]
W/C-ratio	water–cement ratio [–]

Greek symbols

ν	variation coefficient [–]
ν_M	variation coefficient of the measurement method [–]
ν_Z	variation coefficient for ideal random mixture [–]
ρ_B	bulk material density [kg/m^3]
ρ_S	powder density [kg/m^3]
ρ_T	tapped density [kg/m^3]
σ^2	variance [–]
σ_0^2	variance of zero mixture [–]
σ_N	standard stress [N/mm^2]
$\sigma_{Syst.}^2$	systematic variance [–]
σ_M^2	variance of measurement value [–]
σ_Z^2	variance of uniform random mixture [–]
τ_N	shear stress [N/mm^2]
Ψ	sphericity [–]

Acknowledgements

The authors would like to thank the Federal Ministry of Economy and Technology (BMWi) for financial support. The authors furthermore thank Firma ELBA-WERK Maschinen GmbH for initiating the project,

supplying the laboratory single-shaft and laboratory twin-shaft mixer and the experimental product. For the selection of the concrete recipes, advice and assistance, the authors want to thank Prof. Dr.-Ing. Beitzel and associates at the Institute of Construction Methodology and Environmental Technique (IBU) at the Trier Technical College.

Appendix A

Detailed information about the statistical sampling of powder mixtures

The variance $\sigma^2(c_{P,i},t_M)$ is calculated by forming the sum of the deviation squares according to Eq. (3) with the target value concentration $\overline{c_{P,E}}$ for the individual samples N_P, as is also given in Eq. (1). The mixing efficiency then results from the determination of the variance $\sigma^2(c_{P,i},t_M)$, with various mixing times. The variance exists only theoretically because its actual determination requires an infinite number of samples N_P. In practice, only a limited number of samples N_P can be studied. Therefore, the mixing quality is estimated by means of the empirical variance $s^2(c_{P,i},t_M)$, on the basis of the existing analyzed samples. The result of the systematic variance $\sigma^2_{Syst.}$ will be reduced by the mass of individual grain $m_{E,T}$ and sample mass m_P,

$$\sigma^2\left(c_{P,i},t_M\right)\approx s^2\left(c_{P,i},t_M\right)=\frac{1}{N_P}\cdot\sum_{i=1}^{N_P}\left(c_{P,i}-\overline{c_{P,E}}\right)^2 = \sigma_M^2+\sigma_Z^2+\left(1-\frac{m_{E,T}}{m_P}\right)\cdot\sigma^2_{Syst.}. \tag{3}$$

The variation coefficient ν is calculated from the quotient between the square root of the empirical variance according to Eq. (4) and the target value concentration $\overline{c_{P,E}}$ (Eq. (4)),

$$\nu=\frac{s\left(c_{P,i},t_M\right)}{\overline{c_{P,E}}}. \tag{4}$$

The variation coefficient of the ideal random mixture ν_Z is calculated, according to [38], from the mass of the individual particle $m_{E,T}$, the sample quantity m_P, and the target value $\overline{c_{P,E}}$. For particles that do not have a spherical shape and that do not have a monodisperse particle size distribution, Eq. (5) according to *Stange* was modified such that the influence of the distribution and the particle shape is considered. The particularly equal-volume diameters $x_{V,T}$ of the tracer or of the equal-surface diameter $x_{A,T}$ can be determined by simple conversions,

$$\nu_Z=\frac{\sigma_Z}{\overline{c_{P,E}}}=\sqrt{\frac{\left(1-\overline{c_{P,E}}\right)}{\overline{c_{P,E}}}\cdot\frac{m_{E,T}}{m_P}} = \sqrt{\frac{\left(1-\overline{c_{P,E}}\right)}{\overline{c_{P,E}}}\cdot\frac{\rho_S\cdot\frac{1}{6}\cdot\pi\cdot x_{A,T}^2\cdot x_{V,T}\cdot\psi}{m_P}}\approx 6.75\cdot 10^{-6}. \tag{5}$$

The sample quantity m_P can be calculated according to Eq. (6) [39]. This equation consists of the sphericity Ψ, the equal-volume diameter of a sphere x_V, the projected surface of the sample A_P, the powder density ρ_S, and the mass concentration c_j of the individual components j in the powder mixture,

$$m_P=\frac{2}{3}\cdot\rho_P\cdot\sum_{j=1}^{N}A_P\cdot c_j\cdot x_{V,j}\cdot\psi\approx 2.8g. \tag{6}$$

Detailed information about the statistical sampling of powder mixtures by using the image analysis

The variation coefficient of the measurement error ν_M according to Eq. (7) can be determined via a defined sample size A_P, that circumscribes the surface of the largest particle present in the mixture. The segments represent a sample surface A_P, which correspond to $A_P = 15$ pixel·12 pixel in the twin-shaft mixer and $A = 20$ pixel·16 pixel in the single-shaft mixer. The result clearly shows that the measurement error of the variation coefficient dominates the result because the latter is greater than the variation coefficient of the ideal random mixture ν_Z. In determining the variation coefficient ν, one must therefore consider both the variance of the ideal random mixture σ_Z^2 and the variance of the measurement method σ_M^2,

$$\nu_M=\frac{\sigma_M}{\overline{c_{P,E}}}=\frac{A_{E,P}}{A_P}=\frac{1\text{ Pixel}\cdot 1\text{ Pixel}}{15\text{ Pixel}\cdot 12\text{ Pixel}}\approx 5.56\cdot 10^{-3}. \tag{7}$$

The variation coefficient of the so-called zero mixture σ_0^2 according to Eq. (8), a completely de-mixed state of a twin-component mixture, is also calculated from the target value concentration $\overline{c_{P,E}}$,

$$\nu_0=\frac{\sigma_0}{\overline{c_{P,E}}}\sqrt{\frac{\left(1-\overline{c_{P,E}}\right)}{\overline{c_{P,E}}}}\approx 11.83. \tag{8}$$

The shadow formation along the trough edge and in the area of the mixer shaft is not included in the calculations.

Application of the moving average for the power consumption curve

The time series for the moving average value consists of twenty individual values per second. By linear regression according to Eq. (9) of the smoothed measurement values, the particular rise points for a time interval of one second are obtained,

$$P'(t_M)=\frac{\sum\left(\left(t_M-\overline{t}_M\right)\cdot\left(P(t_M)-\overline{P}(t_M)\right)\right)}{\sum\left(t_M-\overline{t}_M\right)^2}. \tag{9}$$

References

[1] M. Pahl, K. Sommer, et al., Mischen von Kunststoff-und Kautschukprodukten, VDI Verlag Kunststofftechnik, ISBN 3-18-234183-9, 1996.
[2] Y. Charonnat, H. Beitzel, Rilem TC 150-ECM Report: efficiency of concrete mixers towards qualification of mixers, Materials and Structures (1997) 28–32.
[3] DIN EN 459-2, Festlegung, Eigenschaften, Herstellung und Konformität, 2002–01.
[4] C.F. Ferraris, Concrete mixing methods and concrete mixers: state of the art, Journal of Research of the National Institute of Standards and Technology 106 (2) (2002) 391–399.
[5] F. Dehn, M. Orgass, Einfluss der Mischtechnik bei Hochleistungsbetonen, Effect of mixing technology on high-performance concretes, AT Aufbereitungstechnik 47 (11) (2006) 32–37.
[6] J.C. Scheydt, G. Herold, H.S. Müller, Ultrahochfester Beton, Symposium Baustoffe und Bauwerkserhaltung in Karlsruhe 3 (2006) 33–44.
[7] L.D. Schwartzentruber, R. Le Roy, J. Cordin, Rheological behaviour of fresh cement pastes formulated from a self compacting concrete (SCC), Cement and Concrete Research 36 (7) (2006) 1203–1213.
[8] M. Schmidt, F. Ekkehard, C. Geisenhanslüke, Ultra High Performance Concrete (UHPC), Kassel university press, ISBN: 978-3-89958-086-0, 2004.
[9] C.F. Ferraris, Measurement of the rheological properties of high performance concrete: state of the art report, Journal of Research of the National Institute of Standards and Technology 104 (5) (1999) 461–478.
[10] S. Diamond, The patch microstructure in concrete: effect of mixing time, Cement and Concrete Research 35 (5) (2005) 1014–1016.
[11] B. Cazacliu, In-mixer measurements for describing mixture evolution during concrete mixing, Chemical Engineering Research and Design 86 (12) (2008) 1423–1433.
[12] B. Cazacliu, J. Legrand, Characterization of the granular-to-fluid state process during mixing by power evolution in a planetary concrete mixer, Chemical Engineering Science 63 (18) (2008) 4617–4630.
[13] B. Cazacliu, N. Roquet, Concrete mixing kinetics by means of power measurement, Cement and Concrete Research 39 (3) (2009) 182–194.
[14] P. Collin, et al., Mixing of concrete or mortars: dispersive aspects, Cement and Concrete Research 37 (9) (2007) 1321–1333.
[15] K. Sommer, Sampling of powders and bulk materials. Verlag Springer Berlin Heidelberg, ISBN-13: 978-3540158912, 1986.
[16] A.D. Fokker, Die mittlere Energie rotierender elektrischer Dipole im Strahlungsfeld, Annalen der Physik 348 (5) (1914) 810–820.

[17] W. Müller, Untersuchung über Mischzeit, Mischgüte und Arbeitsbedarf in Mischtrommeln mit rotierenden Mischelementen, Universität (TH) Karlsruhe, 1966.
[18] K. Sommer, Powder mixing mechanism, Journal of Powder & Bulk Solids Technology 3 (4) (1979) 2–9.
[19] L.T. Fan, et al., Recent developments in solids mixing, Powder Technology 61 (3) (1990) 255–287.
[20] J. Raasch, K. Sommer, Anwendung von statistischen Prüfverfahren im Bereich der Mischtechnik, Chemie-Ingenieur-Technik 62 (1) (1990) 17–22.
[21] R. Holzmüller, Untersuchung zur Schüttgutbewegung beim kontinuierlichen Feststoffmischen, Dissertation Universität Stuttgart, 1984.
[22] A. Merz, Untersuchung zur Axialvermischung in einem kontinuierlich betriebenen Drehrohr mit Isotopenmarkierung, Dissertation Universität (TH) Karlsruhe, 1973.
[23] V. Kehlenbeck, Continuous dynamic mixing of cohesive powders, Dissertation TU München, 2006.
[24] R. Habermann, Untersuchung zur Verknüpfung von Verweilzeit-Verteilung und Mischgüte in einem kontinuierlichen Pflugscharmischer, Dissertation Universität Paderborn, 2005.
[25] F. Landwehr, Entwicklung eines Lichtleiterverfahrens zur Charakterisierung von Mehrphasenströmungen, Dissertation Universität Dortmund, 2005.
[26] P. Eichler, Analyse, Modellierung und Optimierung von Schwerkraftmischern, Dissertation Universität Kaiserslautern, 1998.
[27] C. Wightman, F.J.M., J. Joseph Wilder, A quantitative image analysis method for characterizing mixtures of granular materials, Powder Technology 89 (2) (1996) 165–176.
[28] H. Berthiaux, M.V., L. Tomczak, C. Gatumel, J.F. Demeyre, Principal component analysis for characterising homogeneity in powder mixing using image processing techniques, Chemical Engineering and Processing 45 (5) (2006) 397–403.
[29] B. Daumann, A. Fath, H. Nirschl, Assessment of the efficiency of discontinuous solid mixing by means of image analysis, Chemical Engineering Science 64 (10) (2009) 2320–2331.
[30] H.S. Lee, J.-Y.L., M.Y. Yu, Influence of inorganic pigments on the fluidity of cement mortars, Cement and Concrete Research 35 (4) (2005) 703–710.
[31] H.H. Hausner, Friction conditions in a mass of metal powder, International Journal of Powder Metallurgy 3 (4) (1967) 7–13.
[32] R.L. Carr, Evaluating flow properties of solids, Chemical Engineering 72 (2) 163–168.
[33] D. Schulze, Die Charakterisierung von Schüttgütern für Siloauslegung und Fließfähigkeitsuntersuchungen, The characterization of bulk solids for silo design and folwability test, AT Aufbereitungstechnik 39 (2) (1998) 47–57.
[34] D. Chopin, L.F., B. Cazacliu, Why do HPC and SCC require a longer mixing time? Cement and Concrete Research 34 (12) (2004) 2237–2243.
[35] D. Chopin, B. Cazacliu, F. Larrad de, R. Schell, Monitoring of concrete homogenisation the power consumption curve, Material and Structures 40 (9) (2007) 897–907.
[36] The influence of mixing on the rheology of fresh cement paste. Cement and Concrete Research 29 (12) (1999) 1491–1496.
[37] Bronstejn, Taschenbuch der Mathematik, ISBN 3-8171-2006-0, (2006).
[38] K. Stange, Die Mischgüte einer Zufallsmischung aus drei oder mehr Komponenten, Chemie-Ingenieur-Technik 35 (8) (1963) 331–337.
[39] B. Daumann, H. Nirschl, Assessment of the mixing efficiency of solid mixtures by means of image analysis, Powder Technology 182 (3) (2008) 415–423.